HHS Public Access

Author manuscript

Biol Psychiatry. Author manuscript; available in PMC 2019 June 15.

Published in final edited form as:

Biol Psychiatry. 2018 June 15; 83(12): 1012–1023. doi:10.1016/j.biopsych.2018.01.003.

Glutamatergic Ventral Pallidal Neurons Modulate Activity of the Habenula–Tegmental Circuitry and Constrain Reward Seeking

Jessica Tooley, **Lauren Marconi**, **Jason Alipio**, **Bridget Matikainen-Ankney**, **Polymnia Georgiou**, **Alexxai V. Kravitz**, and **Meaghan C. Creed**

Department of Pharmacology (JT, LM, JA, MCC) and Department of Psychiatry (PG), University of Maryland School of Medicine, Baltimore, and Eating and Addiction Section (BM-A, AVK), National Institute of Digestive and Diabetes and Kidney Diseases, Bethesda, Maryland

Abstract

BACKGROUND—The ability to appropriately integrate and respond to rewarding and aversive stimuli is essential for survival. The ventral pallidum (VP) plays a critical role in processing both rewarding and aversive stimuli. However, the VP is a heterogeneous structure, and how VP subpopulations integrate into larger reward networks to ultimately modulate these behaviors is not known. We identify a noncanonical population of glutamatergic VP neurons that play a unique role in responding to aversive stimuli and constraining inappropriate reward seeking.

METHODS—Using neurochemical, genetic, and electrophysiology approaches, we characterized glutamatergic VP neurons (n = 4–8 mice/group). We performed patch clamp and in vivo electrophysiology recordings in the lateral habenula, rostromedial tegmental nucleus, and ventral tegmental area to determine the effect of glutamatergic VP neuron activation in these target regions (n = 6–10 mice/group). Finally, we selectively optogenetically stimulated glutamatergic VP neurons in a real-time place preference task and ablated these neurons using a virally expressed caspase to determine their necessity for reward seeking.

RESULTS—Glutamatergic VP neurons exhibit little overlap with cholinergic or gamma-aminobutyric acidergic markers, the canonical VP subtypes, and exhibit distinct membrane properties. Glutamatergic VP neurons innervate and increase firing activity of the lateral habenula, rostromedial tegmental nucleus, and gamma-aminobutyric acidergic ventral tegmental area neurons. While nonselective optogenetic stimulation of the VP induced a robust place preference, selective activation of glutamatergic VP neurons induced a place avoidance. Viral ablation of glutamatergic VP neurons increased reward responding and abolished taste aversion to sucrose.

CONCLUSIONS—Glutamatergic VP neurons constitute a noncanonical subpopulation of VP neurons. These glutamatergic VP neurons increase activity of the lateral habenula, rostromedial

Address correspondence to Meaghan C. Creed, Ph.D., Department of Pharmacology, University of Maryland School of Medicine, 655 West Baltimore Street, Room 4-018, Baltimore, MD 21201; mcreed@som.umaryland.edu.

DISCLOSURES

The authors report no biomedical financial interests or potential conflicts of interest.

JT, PG, LM, and MCC performed behavioral experiments. LM, BM-A, JA, MCC, and AVK performed colocalization assays. JA and MCC performed ex vivo physiology. AVK and MCC performed in vivo physiology. MCC designed experiments. JT, JA, MCC, and AVK analyzed data. JT, LM, and MCC wrote the manuscript with input from all authors.

Supplementary material cited in this article is available online at https://doi.org/10.1016/j.biopsych.2018.01.003.

tegmental nucleus, and gamma-aminobutyric acidergic ventral tegmental area neurons and adaptively constrain reward seeking.

Keywords

Aversion; Dopamine (DA); Electrophysiology; Gamma-Aminobutyric acid (GABA); Rostromedial tegmental nucleus (RMTg); Ventral tegmental area (VTA)

Adaptively modulating (1) reward seeking and responding to aversive stimuli are essential to survival. Reward seeking despite negative consequences is a hallmark feature of mood and substance use disorders (2–4). These disorders have been associated with altered activity and function within the reward system, composed of dopamine (DA) neurons in the ventral tegmental area (VTA) and its projections such as the nucleus accumbens (NAc). The ventral pallidum (VP) is a critical node in this network, being a primary output of the NAc (5) and projecting to the VTA, lateral habenula (LHb), and thalamic nuclei (1,6,7). The VP was first identified as a limbic motor interface (8,9) necessary for the expression of motivated behavior and for hedonic processing of reward (6,10). In humans and rodents, the VP is activated in response to cues predicting reward (11–13), while VP lesions decrease reward motivation and hedonic value (14–17). The VP also processes aversive stimuli and has been proposed to integrate positive and negative affective information to guide behavior (18–20). With its central role in the reward network, modulation of the VP has been explored as a therapeutic strategy in psychiatric disease (21). However, to rationally manipulate VP function, comprehensive understanding of its heterogeneity, subcircuitry, and function in reward-related behavior is needed.

The VP is a predominantly gamma-aminobutyric acidergic (GABAergic) nucleus (22) with cholinergic neurons. Within these neurochemical identities, VP neurons exhibit diverse morphological and membrane properties (23,24) as well as mixed electrophysiological responses to rewarding and aversive stimuli, suggesting functional heterogeneity (6). Vesicular glutamate transporter (VGluT2) messenger RNA (mRNA) is expressed in the VP (25,26), although it is unclear whether these VGluT2-positive neurons represent a distinct subclass or whether they overlap with canonical GABAergic or cholinergic neurons. Supporting the idea that subtypes of VP neurons play unique roles in reward-related behavior, it was recently reported that a subset of parvalbumin (PV)-positive VP projection neurons are capable of glutamate co-release and mediate behavioral changes following defeat stress (27). To date, it is not known how the described functional heterogeneity maps onto neurochemically defined populations of VP cells or how populations of glutamatergic VP neurons contribute to the expression of reward-related behavior.

Here, we characterized a glutamatergic subpopulation of VP neurons and investigated how these neurons integrate into the larger reward circuitry. Using patch clamp and in vivo electrophysiology, we showed that activation of glutamatergic VP neurons modulates firing rates of LHb and rostromedial tegmental nucleus (RMTg) neurons as well as GABA and DA neurons in the VTA. Strikingly, while nonspecific optogenetic stimulation of the VP induces a robust place preference, selective stimulation of glutamatergic VP neurons produces behavioral avoidance. Ablation of these neurons revealed their critical role in adaptively

constraining reward seeking. Our results point to the possibility of modulating this population as a therapeutic strategy for disorders of maladaptive reward seeking.

METHODS AND MATERIALS

Animals

Adult male and female VGlut2-IRES-Cre, VGAT-IRES-Cre, ChAT-Cre, PV-Cre, and wild-type littermates on a C57BL/6J background were used (28–30). All procedures were conducted in accordance with the Guide for the Care and Use of Laboratory Animals, as adopted by the National Institutes of Health, and with approval of the Institutional Animal Care and Use Committee at the University of Maryland. (See Supplement for experimental details.)

Stereotaxic Surgery

Adeno-assocated virus–expressing Cre-inducible channelrhodopsin-2 (ChR2)-enhanced yellow fluorescent protein (eYFP), mCherry, rabies virus, or taCasp was bilaterally injected into the VP and expressed for 28 days. Optic fibers, constructed in-house as described previously (31), were implanted bilaterally over the VP and secured with three skull screws and dental cement. Mice with verified viral infection sites and fiber placements in the VP were included in the analyses.

Patch Clamp Electrophysiology

Whole-cell patch clamp recordings were made of the VP, LHb, VTA, and RMTg. Neurons were recorded with cesium-based (voltage clamp) or cesium-free (current clamp) physiological internal solution. Currents were amplified, digitized, and analyzed using a MultiClamp 700B amplifier and Digidata 1440A and Clampex 10.7.0.3 software (Molecular Devices, Sunnyvale, CA).

In Vivo Electrophysiology

Mice were anesthetized, and craniotomies were made over the LHb, VTA, and RMTg. Silicone electrodes (NeuroNexus Technologies, Ann Arbor, MI) were lowered to the recording site. Blue light was delivered to the VP (1-second pulses, 10-second interstimulus interval). Voltage was recorded and analyzed using PlexControl, Offline Sorter, and NeuroExplorer (Plexon, Dallas, TX).

Behavioral Studies

Real-Time Place Preference—Mice were injected with ChR2, and optic fibers were implanted over the VP. Mice were individually run in a behavioral arena with two experimental zones distinguished by floor texture and wall patterns. During the test, 4-ms light pulses were delivered at 1, 10, or 20 Hz when the mice entered the “active” zone; time in zones was analyzed with EthoVision software (Noldus Information Technologies).

Operant Task—Mice were lightly food restricted before training on a fixed ratio (FR)(FR 1, 2, 3) task for sucrose pellets. Following acquisition, mice were tested for 6 days on an FR 5 and three progressive ratio (PR) sessions. Mice were then injected with AAV5-flex-

taCasp-TEV to the VP and allowed 3 days of recovery following surgery. Testing identical to baseline sessions continued for a total of 10 days.

Taste Aversion—During habituation (3 days), mice were water deprived and given 30 minutes to consume tap water in the experimental arena. Water was then replaced with 5% sucrose solution; after 4 days baseline, mice were injected with 0.15 lithium chloride (LiCl) (M) (2% body weight) and were tested the following day. Drinking was recorded using infrared sensors (Arduino).

RESULTS

Glutamatergic VP Neurons Exhibit Distinct Neurochemical and Membrane Properties

We first determined whether glutamatergic VP neurons overlapped with canonical VP subtypes. We injected DIO-mCherry into the VP of *VGluT2-IRES-Cre* mice to visualize glutamatergic neurons (Figure 1A). The VP is predominantly GABAergic, with cholinergic and PV-positive neurons (22,32,33). We immunostained against PV or choline acetyltransferase (ChAT) and quantified overlap with mCherry-expressing neurons. PV was coexpressed in 17.5 ± 2.06% of VGluT2-positive neurons, and the extent of overlap varied as a function of anterior to posterior gradient, with highest colocalization occurring in the anterior VP (anterior 22.6 ± 4.6%, medial 19.7 ± 2.5%, posterior 9.2 ± 2.4%) (Figure 1B). ChAT colabeled with 4.3 ± 1.8% of VGluT2-positive neurons (Figure 1C).

Most VP neurons are GABAergic (12,22). To determine the extent of overlap between VGluT2-positive and GABAergic neurons, we performed fluorescent in situ hybridization to detect Slc17A6 (VGluT2) and Slc31A1 (vesicular GABA transporter [VGAT]) mRNA and quantified overlap of fluorescent signals. Slc31A1 mRNA was observed in very few (1.98 ± 0.66%) Slc17A6-expressing neurons (Figure 1D), suggesting sparse neurons capable of both glutamate and GABA release (Figure 1D).

Having established that glutamatergic VP neurons exhibit low coexpression with markers of canonical VP subtypes, we asked whether these neurons also exhibited distinct membrane properties. We injected DIO-eYFP into the VP of mice expressing Cre− in VGluT2-VGAT-ChAT- or PV-positive neurons and performed patch clamp recordings of genetically identified subtypes (Figure 2A–D). The majority (60%) of GABA neurons could be classified according to published criteria (24,25,34). These GABA neurons were classified as type I based on depolarized membrane potentials (−51.23 ± 2.77 mV) and spontaneous firing (4.78 ± 0.42 Hz), while type II neurons exhibited membrane potentials below −60 mV (−64.46 ± 1.52 mV) and low spontaneous activity (0.47 ± 0.16 Hz). Type I and type II neurons differed in capacitance (type I = 18.6 ± 1.7 pF, type II = 13.4 ± 2.6 pF). Consistent with previous studies, ChAT-positive VP neurons exhibited burst firing with an average firing rate of 2.04 ± 1.0 Hz, large capacitance (32.41 ± 2.15 pF), and resting potential of −58.05 ± 1.79 mV. PV-positive neurons exhibited a membrane capacitance of 17.6 ± 2.3 pF, depolarized membrane potential (−51.33 ± 1.62 mV), and high spontaneous activity (9.77 ± 0.89 Hz). VGluT2-positive VP neurons exhibited small capacitance (14.1 ± 1.3 pF) and low firing rates (0.86 ± 0.75 Hz), similar to type II neurons. However, the resting membrane

potential of VGluT2-positive VP neurons was hyperpolarized (−78.48 ± 2.8 mV), and these neurons were significantly less excitable than all other cell types (Figure 2C).

Glutamatergic VP Neurons Receive Input From Striatum and Amygdala and Innervate the LHb, RMTg, and VTA

Whole-brain scanning was used to detect monosynaptic inputs to glutamatergic VP neurons labeled with pseudorabies virus conjugated to green fluorescent protein (GFP) (Figure 3A). The number of GFP-positive cells was quantified in each upstream brain region [according to the atlas of Paxinos and Franklin (35)], and the number of GFP-positive cells in each brain area was expressed as a proportion of the total GFP-positive cells quantified across all brain regions (Figure 3B). The VP is the primary output of the NAc (36). As predicted from earlier tracing studies (37,38), the majority of GFP-positive cells were concentrated in the NAc shell (20.5 ± 6.2%) and core (9.7 ± 3.7%), and the medial wall of the dorsomedial striatum (9.1 ± 2.0%). A significant proportion of GFP-positive cells were also observed in the central (5.8 ± 1.3%) and medial (9.1 ± 4.3%) subregions of the amygdala. Cortical and midbrain regions were also represented, consistent with the canonical established inputs to the VP (Figure 3B, C and Supplemental Table S1).

For anterograde mapping, we infected glutamatergic cells in the VP with ChR2-eYFP and observed dense fiber labeling in the VTA, LHb, and RMTg (Figure 4A–D). To determine whether glutamatergic VP neurons make functional synapses in these target regions, we performed patch clamp recordings of neurons in the LHb, RMTg, and VTA (DA and GABA neurons). We observed light-evoked excitatory postsynaptic currents (EPSCs) and inhibitory postsynaptic currents (IPSCs) in each neuronal population (Figure 4E). EPSCs were observed in 57.1% (104.9 ± 40.6 pA) of VTA GABA, 64.3% (−113.4 ± 43.4 pA) of VTA DA, 80.0% (−89.7 ± 20.5 pA) of LHb, and 73.3% (−98.6 ± 23.4 pA) of RMTg neurons. IPSCs were less frequent (VTA DA = 42.8%, VTA GABA = 35.7%, LHb = 10.0%, RMTg = 13.3%) and were never observed in the absence of a light-evoked EPSC. There was no difference between areas with respect to proportion of neurons exhibiting light-evoked currents, and EPSCs were observed more frequently than IPSCs.

EPSC paired-pulse ratio (PPR) and IPSC PPR for all regions were calculated (EPSC PPR LHb = 0.72 ± 0.11, RMTg = 0.65 ± 0.12, VTA DA = 0.64 ± 0.09, VTA GABA = 0.69 ± 0.14; IPSC PPR LHb = 0.71 ± 0.26, RMTg = 0.71 ± 0.26, VTA DA = 0.53 ± 0.19, VTA GABA = 0.67 ± 0.22). There was no significant difference in EPSC or IPSC PPR in any region (Figure 4F). We confirmed that EPSCs were blocked by the alpha-amino-3-hydroxy-5-methyl-4-isoxazole propionic acid receptor 6-nitro-7-sulfamobenzoquinoxaline-2-3-dione, while outward IPSCs were blocked by picrotoxin (Figure 4G).

Activation of Glutamatergic Neurons Modulates Firing Activity of LHb, RMTg, and VTA Neurons In Vivo

Our patch clamp physiology results indicate that terminal field activation of glutamatergic VP neurons in the LHb, VTA, and RMTg evokes predominantly EPSCs. However, there is extensive connectivity between these downstream regions; for example, the LHb sends

excitatory afferents to the RMTg, which in turn inhibits DA neurons in the VTA (34,39). Due to this reciprocal connectivity, potential network effects of glutamatergic VP neuron activation on firing rates of these downstream neurons would not be evident in a slice preparation. To determine the effect of glutamatergic VP neuron activation on firing rates, we performed in vivo recording of the LHb, RMTg, and VTA in anesthetized mice and determined the response to activation of glutamatergic VP neurons (Figure 5A, B).

We identified 51 LHb units (4.00 ± 1.60 Hz), 28 of which were significantly modulated by stimulation of glutamatergic VP neurons; of these 28 significantly light-modulated units, all 28 increased their firing rate (Figure 5C). Similarly, we recorded 53 RMTg units (3.79 ± 0.76 Hz), 26 of which were significantly light modulated (Figure 5D); an increased firing rate was observed in nearly all (24/26) units, while a decreased firing rate was observed in the remaining 2 units. Responses in the VTA were more heterogeneous. Of 44 isolated units, 8 were negatively light modulated and 9 were positively light modulated. Of the negatively modulated units, the baseline firing rate was 1.43 ± 0.34 Hz, which decreased by 22.45% in response to light. Of the positively modulated units, the baseline firing rate was 3.76 ± 1.05 Hz and increased by 36.03% in response to light (Figure 5E). There was no difference between animals in terms of baseline (VTA DA: $F_2 = 1.897$, $p = .244$; VTA GABA: $F_2 = 0.799$, $p = .500$, LHb: $F_2 = 1.58$, $p = .225$; RMTg: $F_2 = 0.826$, $p = .450$) or light-evoked change in firing (VTA DA: $F_2 = 1.500$, $p = .296$; VTA GABA: $F_2 = 0.572$, $p = .593$; LHb: $F_2 = 0.540$, $p = .589$; RMTg: $F_2 = 1.533$, $p = .237$). We compared the variability in latency to peak change in firing rate for each unit (Supplemental Figure S1). There was no significant difference in the latency to peak change in firing rate or in variance to peak firing rate between brain areas, nor was there a significant relationship between latency to peak change and magnitude of peak change in firing rate. In the temporal cortex, a control region that does not receive input from the VP, there was no significant modulation of local field potential response or of spiking activity of any of the seven identified units (Supplemental Figure S2).

Glutamatergic VP Neurons Constrain Reward Seeking and Contribute to Aversion Learning

We nonselectively stimulated VP neurons in a real-time place preference task (Figure 6A–C). Mice expressing ChR2 but not eYFP exhibited a robust preference for the stimulation (stim)-paired side (ChR2: baseline 51.1 ± 1.4%, stim 77.1 ± 4.9%; eYFP: baseline 49.7 ± 1.7, stim 47.0 ± 5.1%) (Figure 6D). Stimulation of glutamatergic VP neurons at 20 Hz induced place aversion (baseline 49.9 ± 2.8%, stim 23.1 ± 6.3%) (Figure 6E, F), while Cre-negative mice that did not express the optogenetic effector showed no preference or avoidance of the stimulation-paired side (baseline 53.1 ± 2.5%, stim 52.8 ± 3.1%) (Figure 6E, F). Simulation of 10 Hz (change from baseline: −22.55 ± 3.19%, $t = 7.058$, $p = .006$) but not 1 Hz (change from baseline: 7.80 ± 7.18%, $t = 1.087$, $p = .357$) induced real-time place avoidance.

To interrogate the role of glutamatergic VP neurons in reward seeking and motivation, we trained mice on an operant reward task before selective ablation of glutamatergic VP neurons with AAV2-flex-taCasp3-TEVp. Mice first learned an FR task where lever presses were rewarded with a sucrose pellet (Figure 7A). There was no effect of genotype on the

initial acquisition of the FR responding task (Figure 7B). There was no effect of taCasp3 lesion on number lever presses made in the FR task (Cre− = pre 197.83 ± 9.5, post 264.13 ± 12.4 presses/session; Cre+ = pre 183.78 ± 10.65, post 214.53 ± 10.8 presses/session) (Figure 7C); however, there was a significant increase in rate of responding in taCasp3-lesioned mice (Cre− = pre 36.09 ± 1.9, post 39.36 ± 2.54 min/session; Cre+ = pre 36.12 ± 2.6, post 22.04 ± 2.31 min/session) (Figure 7D). Following taCasp3 lesion, the number of lever presses in the PR task increased (Cre− = pre 372.11 ± 28.14, post 443.39 ± 32.9 presses/session; Cre+ = pre 496.24 ± 48.87, post 1656.62 ± 444.88 presses/session), as did the breakpoint (Cre− = pre 14.47 ± 0.38, post 15.0 ± 0.41; Cre+ = pre 15.2 ± 0.3, post 19.0 ± 0.42; $F_{\text{session} \times \text{genotype}} = 5.09$, $p = .001$) (Figure 7E) and time of active lever pressing during the session ($F_{\text{genotype}} = 245.011$, $p < .001$; $F_{\text{session} \times \text{genotype}} = 4.727$, $p = .026$).

In a sucrose aversion task, mice with taCasp3 lesions or controls were allowed free access to 5% sucrose solution. After sucrose intake stabilized over 4 days, mice were injected with LiCl and testing was conducted identically the following day (Figure 7F). Baseline drinking time was higher in taCasp-lesioned mice relative to control mice, consistent with their increased responding and higher breakpoint in the operant task. As previously reported (35), LiCl injection significantly reduced sucrose consumption in control mice (50.3 ± 11.1% decrease from baseline). However, mice with taCasp lesions of glutamatergic VP neurons showed no change in sucrose consumption following LiCl injection (31.4 ± 9.4% nonsignificant change) (Figure 7G). There were no differences in spontaneous locomotor activity in an open field task between unlesioned mice (82.74 ± 20.83 m) and lesioned mice (77.7 ± 17.53 m) (Figure 7I).

DISCUSSION

The VP is a critical region for the expression of motivated behavior and for processing rewarding and aversive stimuli. Dissecting the heterogeneity of the VP is essential for understanding how the VP contributes to coordinating behavioral responses to rewarding and aversive stimuli and is necessary for understanding reward seeking in adaptive and pathological states. Glutamatergic VP neurons overlap minimally with GABAergic or cholinergic cell markers (Figure 1). Analogous to the external globus pallidus, the VP has been reported to contain PV-positive projection neurons (36), some of which are capable of glutamate release (27). We found that PV-positive neurons accounted for only a small proportion (17.5%) of glutamatergic neurons; the majority of glutamatergic VP neurons did not colocalize with PV. Likewise, only a small proportion of PV-positive VP neurons express VGluT2 [19.5% (27)]. Electrophysiological measurement of membrane properties further indicate that glutamatergic neurons are a distinct subclass; VGluT2-positive neurons exhibited a hyperpolarized membrane potential relative to previously categorized GABAergic or cholinergic neurons (Figure 2). While our immunohistochemistry results indicated a small overlap between glutamatergic and PV-positive neurons, our recording from identified PV-positive neurons consistently found slightly depolarized membrane potentials and high rates of spontaneous firing (Figure 2), unlike the hyperpolarized potential and lack of spontaneous firing observed in the identified VGluT2-positive population. One possibility is that our recordings of identified VGluT2-positive neurons did not sample from the small subpopulation that coexpresses PV. Future studies will elucidate

whether there are meaningful functional properties of the subpopulation of VP neurons that coexpress PV and VGluT2. These results indicate that glutamatergic neurons constitute a subclass distinct from classically described VP cell types.

Given their unique neurochemical and electrophysiological identity, we next asked whether glutamatergic neurons exhibited unique afferent and efferent connections relative to classical VP subtypes. Consistent with early tracing studies of inputs to the VP (5,36,37), our pseudorabies tracing revealed monosynaptic inputs to glutamatergic VP neurons arising predominantly from the NAc but also from cortical and amygdala regions (Figure 3 and Supplemental Table S1). Our study did not determine the neurochemical identity of these upstream projections, although functional in vivo electrophysiology studies have determined that inputs from the NAc are GABAergic, projections from cortical and amygdala regions are glutamatergic (39), and inputs arising from the VTA are an important source of DA to the VP (40). Patch clamp recordings in the terminal fields of glutamatergic VP neurons revealed primarily monosynaptic, light-evoked EPSCs in the LHb, RMTg, and VTA (Figure 4). In the VTA, we used electrophysiological criteria (capacitance > 30 pF and presence of a depolarization-activated inward current) to classify neurons as putative DA or GABA (41,42). Our complementary in vivo recordings in anesthetized mice (Figure 5) revealed that optogenetic activation of glutamatergic VP neurons significantly increased firing rates of LHb and RMTg neurons, while effects in the VTA were more complex. In the VTA, half of the modulated single units were increased, while the other half were decreased. Of the positively modulated units, all exhibited a narrow waveform and the average basal firing rate was 3.8 Hz. All negatively modulated units exhibited a longer triphasic waveform and a lower basal firing rate (1.4 Hz). These criteria have been classically used to define neurons as GABA or DA (43). Both ex vivo and in vivo recordings were performed in the lateral VTA, where classical electrophysiological criteria can usefully distinguish between GABA and DA cell types (44). However, we cannot exclude the possibility that some of the putative GABAergic neurons we recorded are DA neurons that lack an inward current and exhibit smaller capacitance values (45,46). Inhibition of the pallidum has been shown to increase the proportion of spontaneously active VTA DA neurons through a disinhibition mechanism (47,48). Our results are consistent with this interpretation and also suggest that inhibition of this minority of glutamatergic VP neurons may participate in this disinhibition indirectly through relieving the excitatory drive on LHb, RMTg, and VTA GABA neurons.

According to models of input–output relationships of the VTA (45,49), the putative VTA DA neurons we recorded project to the NAc; a decrease in DA firing and consequent decrease in DA release in the NAc would reduce the likelihood of repeating actions that lead to that outcome. Based on these network effects, we hypothesized that activation of glutamatergic VP neurons would result in behavioral avoidance response to stimulation. Strikingly, while nonspecific stimulation of the VP produced robust place preference, consistent with the reinforcing properties of VP stimulation in intracranial self-stimulation studies (50,51), selective stimulation of glutamatergic VP neurons induced a real-time avoidance of stimulation (Figure 6). This indicates that glutamatergic VP neurons are situated to play a unique role in reward-related behavior. Given that VP lesions decrease reward motivation (15,16,21), we asked whether selective lesions of glutamatergic VP neurons would have the opposing effect. Virally mediated caspase ablation of glutamatergic VP neurons increased

the rate of responding for sucrose and enhanced motivation for sucrose in a PR task (Figure 7). Finally, we asked whether glutamatergic VP neurons are necessary for adaptively constraining reward seeking by testing the avoidance response to sucrose paired with LiCl. We found that ablation of glutamatergic VP neurons rendered mice insensitive to sucrose devaluation with LiCl, further supporting the idea that glutamatergic VP neurons adaptively constrain reward seeking. In addition to this role in constraining reward seeking, future work will determine whether activity of glutamatergic VP neurons alters reward thresholds or contributes to behavioral responses to aversive stimuli beyond the context of reward seeking.

Substance use and mood disorders are characterized by maladaptive reward seeking. The VP is a central node in the reward system, with reciprocal projections with the NAc, cortex, habenula, and midbrain structures, all of which show altered activation during symptoms of bipolar disorder and in response to drug-associated cues (52–54). Nonoverlapping populations of VP efferents (i.e., projections to the subthalamic nucleus and VTA) are activated in response to drug-associated cues, and activity contributes to reinstatement of drug seeking (55,56). Mahler and colleagues proposed that glutamatergic efferents from the VP to the VTA did not modulate VTA DA neuron activity in slice and did not contribute to drug reinstatement (56). Our results support this interpretation. Our slice results showed mixed EPSCs and IPSCs onto VTA DA neurons from glutamatergic VP efferents, while in vivo recordings, in which network connectivity is preserved, revealed a predominant inhibitory effect of glutamatergic VP neuron activation on the VTA DA neuron firing rate. Earlier work demonstrated that the RTMg is activated by aversive stimuli and its activity inhibits VTA DA neurons (57), while activation of LHb projections to the VTA and RMTg is sufficient to induce behavioral aversion (58). Our work extends these findings by identifying and characterizing a discrete population of glutamatergic VP neurons that modulate activity of the VTA directly and indirectly through polysynaptic effects on LHb and RMTg circuitry. While our study did not determine whether the glutamatergic VP neurons projecting to the LHb, VTA, and RMTg are distinct populations, our in vivo results suggest that effects of glutamatergic VP neuron activation on activity of the interconnected habenula and tegmental circuitry, rather than activity of one specific efferent population, mediate behavioral avoidance and constraint of reward seeking.

The ability to upregulate activity of glutamatergic VP neurons in response to cues triggering inappropriate reward seeking could have potential to inhibit maladaptive reward seeking in psychiatric disorders. For example, pallidal structures have been shown to be architecturally safe targets for deep brain stimulation in humans and in animal models (59,60), and advances in region- and cell-type-specific drug delivery may soon provide strategies to target VP subpopulations pharmacologically (61–63). Future work will be needed to leverage the unique electrophysiological and genetic properties of glutamatergic VP neurons as a potential treatment strategy for disorders of maladaptive reward seeking.

Supplementary Material

Refer to Web version on PubMed Central for supplementary material.

Acknowledgments

This work was supported by the National Institute of Digestive and Diabetes and Kidney Diseases Intramural Research Program (to AVK) and internal funds from the University of Maryland School of Medicine (to MCC).

We thank M.J. Krashes for assistance with rabies virus constructs.

References

1. Haber SN, Groenewegen HJ, Grove EA, Nauta WJ. Efferent connections of the ventral pallidum: Evidence of a dual striato pallidofugal pathway. J Comp Neurol. 1985; 235:322–335. [PubMed: 3998213]
2. Dichter GS, Damiano CA, Allen JA. Reward circuitry dysfunction in psychiatric and neurodevelopmental disorders and genetic syndromes: Animal models and clinical findings. J Neurodev Disord. 2012; 4:19. [PubMed: 22958744]
3. Nusslock R, Alloy LB. Reward processing and mood-related symptoms: An RDoC and translational neuroscience perspective. J Affect Disord. 2017; 216:3–16. [PubMed: 28237133]
4. Feil J, Sheppard D, Fitzgerald PB, Yucel M, Lubman DI, Bradshaw JL. Addiction, compulsive drug seeking, and the role of frontostriatal mechanisms in regulating inhibitory control. Neurosci Biobehav Rev. 2010; 35:248–275. [PubMed: 20223263]
5. O'Donnell P, Lavin A, Enquist LW, Grace AA, Card JP. Interconnected parallel circuits between rat nucleus accumbens and thalamus revealed by retrograde transynaptic transport of pseudorabies virus. J Neurosci. 1997; 17:2143–2167. [PubMed: 9045740]
6. Root DH, Melendez RI, Zaborszky L, Napier TC. The ventral pallidum: Subregion-specific functional anatomy and roles in motivated behaviors. Prog Neurobiol. 2015; 130:29–70. [PubMed: 25857550]
7. Young WS 3rd, Alheid GF, Heimer L. The ventral pallidal projection to the mediodorsal thalamus: A study with fluorescent retrograde tracers and immunohistofluorescence. J Neurosci. 1984; 4:1626–1638. [PubMed: 6374062]
8. Yim CY, Mogenson GJ. Response of ventral pallidal neurons to amygdala stimulation and its modulation by dopamine projections to nucleus accumbens. J Neurophysiol. 1983; 50:148–161. [PubMed: 6875644]
9. Mogenson GJ, Jones DL, Yim CY. From motivation to action: Functional interface between the limbic system and the motor system. Prog Neurobiol. 1980; 14:69–97. [PubMed: 6999537]
10. Kalivas PW, Volkow ND. The neural basis of addiction: A pathology of motivation and choice. Am J Psychiatry. 2005; 162:1403–1413. [PubMed: 16055761]
11. Young KA, Franklin TR, Roberts DC, Jagannathan K, Suh JJ, Wetherill RR, et al. Nipping cue reactivity in the bud: Baclofen prevents limbic activation elicited by subliminal drug cues. J Neurosci. 2014; 34:5038–5043. [PubMed: 24695721]
12. Root DH, Ma S, Barker DJ, Megehee L, Striano BM, Ralston CM, et al. Differential roles of ventral pallidum subregions during cocaine self-administration behaviors. J Comp Neurol. 2013; 521:558–588. [PubMed: 22806483]
13. Tindell AJ, Smith KS, Pecina S, Berridge KC, Aldridge JW. Ventral pallidum firing codes hedonic reward: When a bad taste turns good. J Neurophysiol. 2006; 96:2399–2409. [PubMed: 16885520]
14. Cromwell HC, Berridge KC. Where does damage lead to enhanced food aversion: The ventral pallidum/substantia innominata or lateral hypothalamus? Brain Res. 1993; 624:1–10. [PubMed: 8252379]
15. Shimura T, Imaoka H, Yamamoto T. Neurochemical modulation of ingestive behavior in the ventral pallidum. Eur J Neurosci. 2006; 23:1596–1604. [PubMed: 16553623]
16. Miller JM, Vorel SR, Tranguch AJ, Kenny ET, Mazzoni P, van Gorp WG, et al. Anhedonia after a selective bilateral lesion of the globus pallidus. Am J Psychiatry. 2006; 163:786–788. [PubMed: 16648316]
17. Farrar AM, Font L, Pereira M, Mingote S, Bunce JG, Chrobak JJ, et al. Forebrain circuitry involved in effort-related choice: Injections of the $GABA_A$ agonist muscimol into ventral pallidum

alter response allocation in food-seeking behavior. Neuroscience. 2008; 152:321–330. [PubMed: 18272291]

18. Itoga CA, Berridge KC, Aldridge JW. Ventral pallidal coding of a learned taste aversion. Behav Brain Res. 2016; 300:175–183. [PubMed: 26615907]
19. Creed M, Ntamati NR, Chandra R, Lobo MK, Luscher C. Convergence of reinforcing and anhedonic cocaine effects in the ventral pallidum. Neuron. 2016; 92:214–226. [PubMed: 27667004]
20. Saga Y, Richard A, Sgambato-Faure V, Hoshi E, Tobler PN, Tremblay L. Ventral pallidum encodes contextual information and controls aversive behaviors. Cereb Cortex. 2017; 27:2528–2543. [PubMed: 27114173]
21. Napier TC, Mickiewicz AL. The role of the ventral pallidum in psychiatric disorders. Neuropsychopharmacology. 2010; 35:337.
22. Fallon JH, Loughlin SE, Ribak CE. The islands of Calleja complex of rat basal forebrain: III. Histochemical evidence for a striatopallidal system. J Comp Neurol. 1983; 218:91–120. [PubMed: 6136533]
23. Bengtson CP, Lee DJ, Osborne PB. Opposing electrophysiological actions of 5-HT on noncholinergic and cholinergic neurons in the rat ventral pallidum in vitro. J Neurophysiol. 2004; 92:433–443. [PubMed: 14960557]
24. Kupchik YM, Kalivas PW. The rostral subcommissural ventral pallidum is a mix of ventral pallidal neurons and neurons from adjacent areas: An electrophysiological study. Brain Struct Funct. 2013; 218:1487–1500. [PubMed: 23143342]
25. Geisler S, Derst C, Veh RW, Zahm DS. Glutamatergic afferents of the ventral tegmental area in the rat. J Neurosci. 2007; 27:5730–5743. [PubMed: 17522317]
26. Hur EE, Zaborszky L. Vglut2 afferents to the medial prefrontal and primary somatosensory cortices: A combined retrograde tracing in situ hybridization study [corrected]. J Comp Neurol. 2005; 483:351–373. [PubMed: 15682395]
27. Knowland D, Lilascharoen V, Pacia CP, Shin S, Wang EH, Lim BK. Distinct ventral pallidal neural populations mediate separate symptoms of depression. Cell. 2017; 170:284–297. [PubMed: 28689640]
28. Vong L, Ye C, Yang Z, Choi B, Chua S Jr, Lowell BB. Leptin action on GABAergic neurons prevents obesity and reduces inhibitory tone to POMC neurons. Neuron. 2011; 71:142–154. [PubMed: 21745644]
29. Rossi J, Balthasar N, Olson D, Scott M, Berglund E, Lee CE, et al. Melanocortin-4 receptors expressed by cholinergic neurons regulate energy balance and glucose homeostasis. Cell Metab. 2011; 13:195–204. [PubMed: 21284986]
30. Tanahira C, Higo S, Watanabe K, Tomioka R, Ebihara S, Kaneko T, et al. Parvalbumin neurons in the forebrain as revealed by parvalbumin-Cre transgenic mice. Neurosci Res. 2009; 63:213–223. [PubMed: 19167436]
31. Sparta DR, Stamatakis AM, Phillips JL, Hovelso N, van Zessen R, Stuber GD. Construction of implantable optical fibers for long-term optogenetic manipulation of neural circuits. Nat Protoc. 2011; 7:12–23. [PubMed: 22157972]
32. Bengtson CP, Osborne PB. Electrophysiological properties of cholinergic and noncholinergic neurons in the ventral pallidal region of the nucleus basalis in rat brain slices. J Neurophysiol. 2000; 83:2649–2660. [PubMed: 10805665]
33. Gielow MR, Zaborszky L. The input–output relationship of the cholinergic basal forebrain. Cell Rep. 2017; 18:1817–1830. [PubMed: 28199851]
34. Yetnikoff L, Cheng AY, Lavezzi HN, Parsley KP, Zahm DS. Sources of input to the rostromedial tegmental nucleus, ventral tegmental area, and lateral habenula compared: A study in rat. J Comp Neurol. 2015; 523:2426–2456. [PubMed: 25940654]
35. Yasoshima Y, Shimura T. Midazolam impairs the retrieval of conditioned taste aversion via opioidergic transmission in mice. Neurosci Lett. 2017; 636:64–69. [PubMed: 27984199]
36. Gaykema RP, Zaborszky L. Parvalbumin-containing neurons in the basal forebrain receive direct input from the substantia nigra-ventral tegmental area. Brain Res. 1997; 747:173–179. [PubMed: 9042545]

37. Sesack SR, Deutch AY, Roth RH, Bunney BS. Topographical organization of the efferent projections of the medial prefrontal cortex in the rat: An anterograde tract-tracing study with *Phaseolus vulgaris* leucoagglutinin. J Comp Neurol. 1989; 290:213–242. [PubMed: 2592611]
38. Napier TC, Mitrovic I. Opioid modulation of ventral pallidal inputs. Ann N Y Acad Sci. 1999; 877:176–201. [PubMed: 10415650]
39. Maroteaux M, Mameli M. Cocaine evokes projection-specific synaptic plasticity of lateral habenula neurons. J Neurosci. 2012; 32:12641–12646. [PubMed: 22956853]
40. Maslowski-Cobuzzi RJ, Napier TC. Activation of dopaminergic neurons modulates ventral pallidal responses evoked by amygdala stimulation. Neuroscience. 1994; 62:1103–1119. [PubMed: 7845589]
41. Mercuri NB, Bonci A, Calabresi P, Stefani A, Bernardi G. Properties of the hyperpolarization-activated cation current I_h in rat midbrain dopaminergic neurons. Eur J Neurosci. 1995; 7:462–469. [PubMed: 7773443]
42. Steffensen SC, Svingos AL, Pickel VM, Henriksen SJ. Electrophysiological characterization of GABAergic neurons in the ventral tegmental area. J Neurosci. 1998; 18:8003–8015. [PubMed: 9742167]
43. Ungless MA, Grace AA. Are you or aren't you? Challenges associated with physiologically identifying dopamine neurons. Trends Neurosci. 2012; 35:422–430. [PubMed: 22459161]
44. Chieng B, Azriel Y, Mohammadi S, Christie MJ. Distinct cellular properties of identified dopaminergic and GABAergic neurons in the mouse ventral tegmental area. J Physiol. 2011; 589:3775–3787. [PubMed: 21646409]
45. Lammel S, Lim BK, Ran C, Huang KW, Betley MJ, Tye KM, et al. Input-specific control of reward and aversion in the ventral tegmental area. Nature. 2012; 491:212–217. [PubMed: 23064228]
46. Margolis EB, Lock H, Hjelmstad GO, Fields HL. The ventral tegmental area revisited: Is there an electrophysiological marker for dopaminergic neurons? J Physiol. 2006; 577:907–924. [PubMed: 16959856]
47. Lisman JE, Grace AA. The hippocampal-VTA loop: Controlling the entry of information into long-term memory. Neuron. 2005; 46:703–713. [PubMed: 15924857]
48. Floresco SB, West AR, Ash B, Moore H, Grace AA. Afferent modulation of dopamine neuron firing differentially regulates tonic and phasic dopamine transmission. Nat Neurosci. 2003; 6:968–973. [PubMed: 12897785]
49. Ikemoto S. Dopamine reward circuitry: Two projection systems from the ventral midbrain to the nucleus accumbens-olfactory tubercle complex. Brain Res Rev. 2007; 56:27–78. [PubMed: 17574681]
50. Burgdorf J, Wood PL, Kroes RA, Moskal JR, Panksepp J. Neurobiology of 50-kHz ultrasonic vocalizations in rats: Electrode mapping, lesion, and pharmacology studies. Behav Brain Res. 2007; 182:274–283. [PubMed: 17449117]
51. Panagis G, Spyraki C. Neuropharmacological evidence for the role of dopamine in ventral pallidum self-stimulation. Psychopharmacology (Berl). 1996; 123:280–288. [PubMed: 8833421]
52. Sharma A, Wolf DH, Ciric R, Kable JW, Moore TM, Vandekar SN, et al. Common dimensional reward deficits across mood and psychotic disorders: A connectome-wide association study. Am J Psychiatry. 2017; 174:657–666. [PubMed: 28135847]
53. Li Q, Li W, Wang H, Wang Y, Zhang Y, Zhu J, et al. Predicting subsequent relapse by drug-related cue-induced brain activation in heroin addiction: An event-related functional magnetic resonance imaging study. Addict Biol. 2015; 20:968–978. [PubMed: 25214465]
54. Mason L, O'Sullivan N, Montaldi D, Bentall RP, El-Deredy W. Decision-making and trait impulsivity in bipolar disorder are associated with reduced prefrontal regulation of striatal reward valuation. Brain. 2014; 137:2346–2355. [PubMed: 25009169]
55. Prasad AA, McNally GP. Ventral pallidum output pathways in context-induced reinstatement of alcohol seeking. J Neurosci. 2016; 36:11716–11726. [PubMed: 27852779]
56. Mahler SV, Vazey EM, Beckley JT, Keistler CR, McGlinchey EM, Kaufling J, et al. Designer receptors show role for ventral pallidum input to ventral tegmental area in cocaine seeking. Nat Neurosci. 2014; 17:577–585. [PubMed: 24584054]

57. Jhou TC, Fields HL, Baxter MG, Saper CB, Holland PC. The rostromedial tegmental nucleus (RMTg), a GABAergic afferent to midbrain dopamine neurons, encodes aversive stimuli and inhibits motor responses. Neuron. 2009; 61:786–800. [PubMed: 19285474]
58. Stamatakis AM, Stuber GD. Activation of lateral habenula inputs to the ventral midbrain promotes behavioral avoidance. Nat Neurosci. 2012; 15:1105–1107. [PubMed: 22729176]
59. Welter ML, Grabli D, Vidailhet M. Deep brain stimulation for hyperkinetics disorders: Dystonia, tardive dyskinesia, and tics. Curr Opin Neurol. 2010; 23:420–425. [PubMed: 20610993]
60. Yu W, Walling I, Smith AB, Ramirez-Zamora A, Pilitsis JG, Shin DS. Deep brain stimulation of the ventral pallidum attenuates epileptiform activity and seizing behavior in pilocarpine-treated rats. Brain Stimul. 2016; 9:285–295. [PubMed: 26723019]
61. Shields BC, Kahuno E, Kim C, Apostolides PF, Brown J, Lindo S, et al. Deconstructing behavioral neuropharmacology with cellular specificity. Science. 2017; 356:eaaj2161. [PubMed: 28385956]
62. Airan RD, Meyer RA, Ellens NP, Rhodes KR, Farahani K, Pomper MG, et al. Noninvasive targeted transcranial neuromodulation via focused ultrasound gated drug release from nanoemulsions. Nano Lett. 2017; 17:652–659. [PubMed: 28094959]
63. Vazey EM, Aston-Jones G. Designer receptors: Therapeutic adjuncts to cell replacement therapy in Parkinson's disease. J Clin Invest. 2014; 124:2858–2860. [PubMed: 24937425]

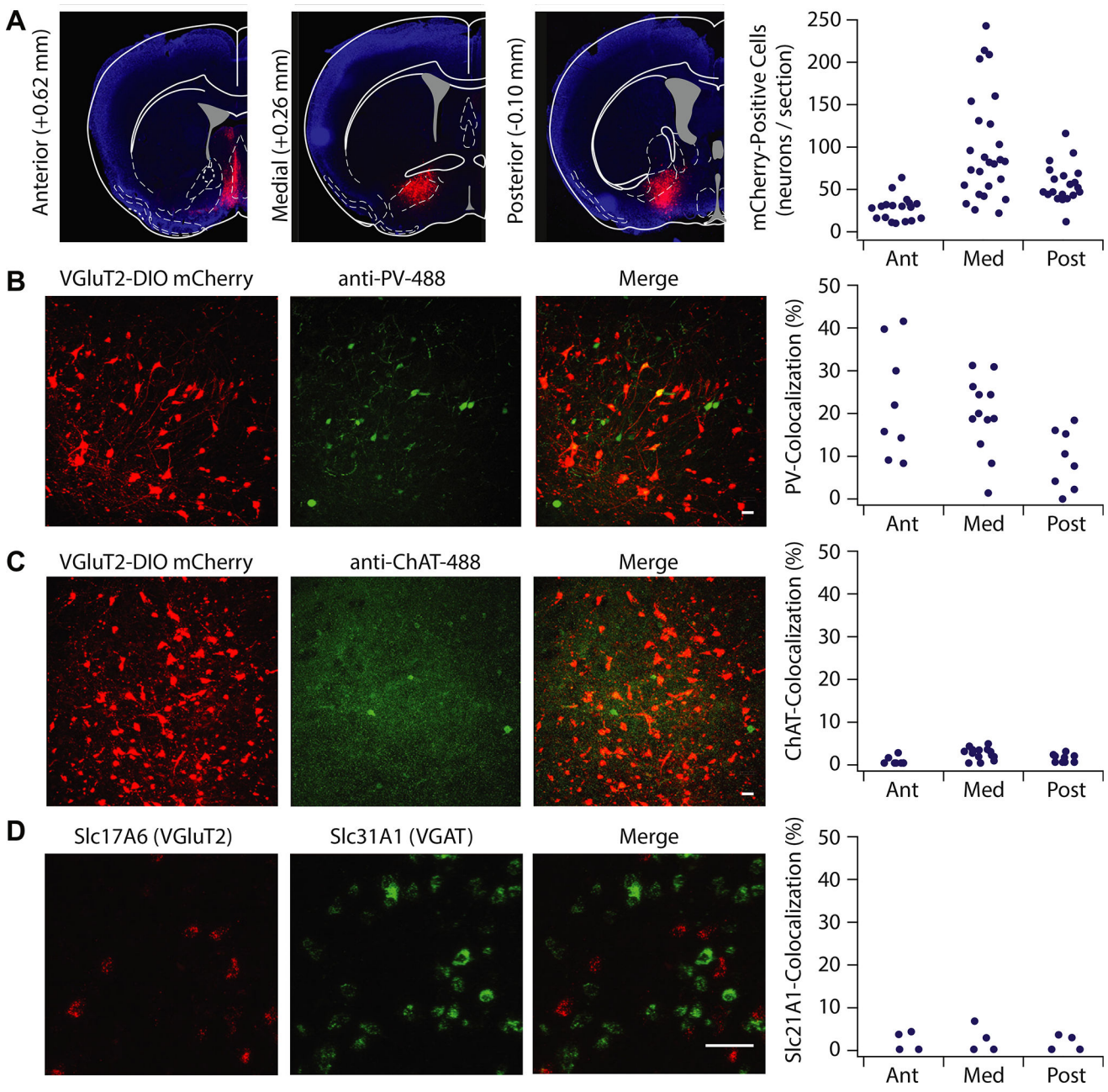

Figure 1.

Vesicular glutamate transporter (VGluT2)-positive ventral pallidum (VP) neurons exhibit distinct neurochemical properties from canonical VP subtypes. **(A)** VGluT2-Cre mice were injected with floxed mCherry in the VP to selectively label VGluT2-positive VP cells. VGluT2-positive VP neurons were expressed through the anterior (Ant) (+0.98 to 0.50 mm anterior–posterior relative to bregma; 27.6 ± 3.4 cells/section), medial (Med) (+0.50 to 0.02 mm anterior–posterior relative to bregma; 97.4 ± 11.8 cells/section), and posterior (Post) (0.02 to −0.46 mm anterior–posterior relative to bregma; 55.2 ± 5.6 cells/section) planes of the VP. To measure the percentage of selectively labeled glutamatergic neurons that colocalize with parvalbumin (PV) and choline acetyltransferase (ChAT), confocal images

(20×) were taken of VP sections of VGluT2-Cre mice infected with floxed mCherry and immunostained against PV and ChAT primary antibodies, with the secondary antibody conjugated to Alexa Fluor 488. **(B)** Colocalization of PV and mCherry was observed in the anterior (22.6 ± 4.6%), medial (19.7 ± 2.5%), and posterior (9.2 ± 2.4%) planes, with highest colocalization occurring in the anterior VP (F_2 = 4.178, p = .027). **(C)** ChAT and mCherry exhibited little coexpression (anterior 7.4 ± 5.0%, medial 3.3 ± 0.5%, posterior 2.89 ± 0.59%; F_2 = 1.780, p = .183). **(D)** Fluorescent images and quantification of in situ hybridization against VGluT2 (Slc17A6, red) and VGAT (Slc31A1, green) revealed low colocalization of VGluT and VGAT cells throughout the VP (anterior 2.0 ± 1.2%, medial 2.3 ± 1.6%, posterior 2.1 ± 1.1%; F_2 = 0.100, p = .906). Scale bars: 50 μM. VGAT, vesicular GABA transporter.

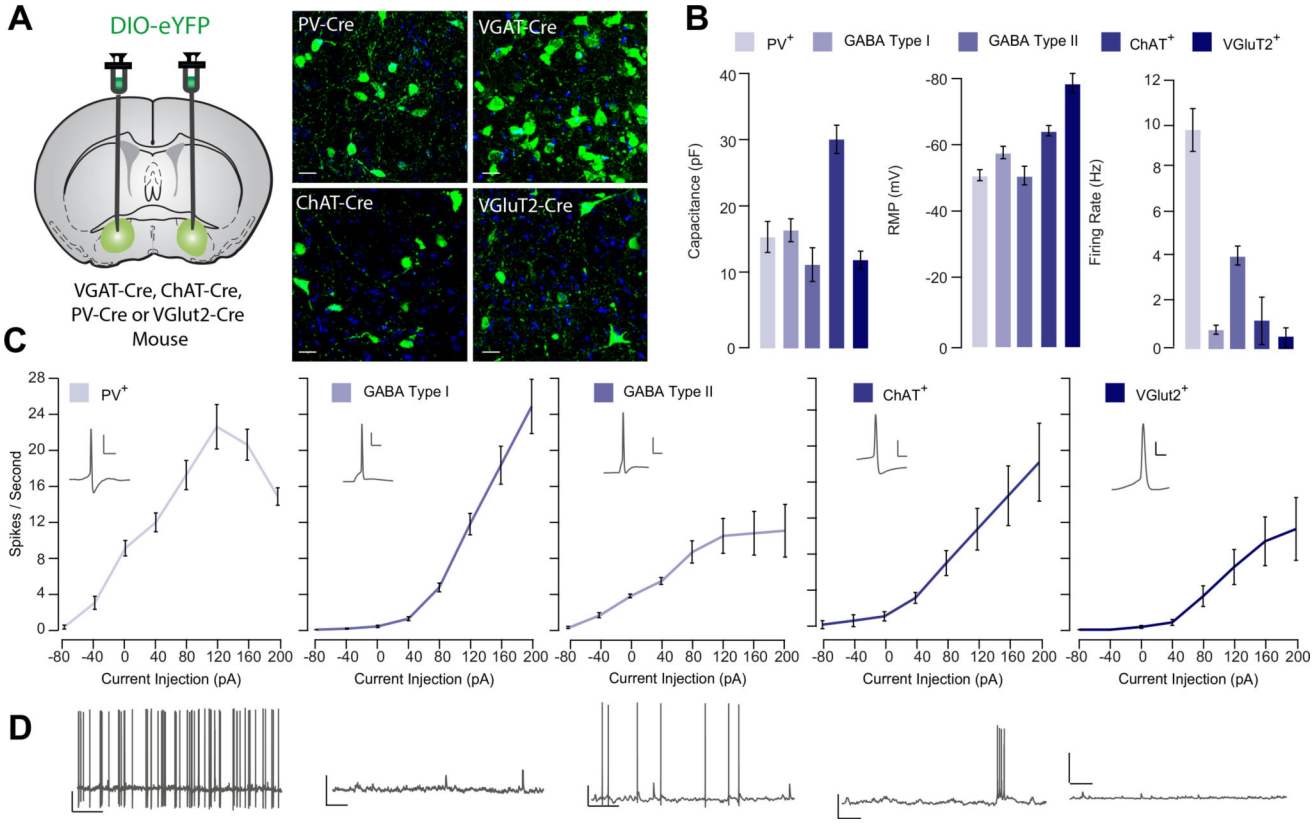

Figure 2.

Vesicular glutamate transporter (VGluT2)-positive ventral pallidum (VP) neurons exhibit distinct membrane properties from canonical VP subtypes. **(A)** Experimental schematic. Floxed adeno-associated virus construct encoding enhanced yellow fluorescent protein (eYFP) was injected into the VP of VGAT-Cre, ChAT-Cre, PV-Cre, or VGluT2-Cre mice to selectively label genetically defined cell types in the VP. Using patch clamp electrophysiology, passive membrane properties were measured from parvalbumin (PV)-positive (PV+; $n = 11$), gamma-aminobutyric acid (GABA) type I ($n = 14$), and GABA type II ($n = 14$), choline acetyltransferase (ChAT)-positive (ChAT+; $n = 8$), and VGluT2-expressing (VGluT2+; $n = 7$) VP neurons. **(B)** Summary of average capacitance values (PV+ = 17.6 ± 2.3 pF, GABA I = 18.6 ± 1.7 pF, GABA II = 13.4 ± 2.6 pF, ChAT+ = 32.4 ± 2.1 pF, VGluT+ = 14.1 ± 1.3 pF), resting membrane potential (PV+ = −51.3 ± 1.6 mV, GABA I = −64.5 ± 1.5 mV, GABA II = −51.2 ± 2.8 mV, ChAT+ = −58.1 ± 1.8 mV, VGluT+ = −78.5 ± 2.8 mV), and firing rate (PV+ = 9.77 ± 0.89 Hz, GABA I = 0.47 ± 0.16 Hz, GABA II = 4.78 ± 0.42 Hz, ChAT+ = 2.03 ± 1.00 Hz, VGluT+ = 0.86 ± 0.75 Hz) is shown for each genetically defined population of VP neurons. VGluT+ VP neurons were significantly hyperpolarized, $F_4 = 27.24$ $p < .001$, Tukey post hoc tests for comparison of VGluT against all other populations < .01. **(C)** For each genetically identified cell population, the number of action potentials per second in response to successive current injection (−40 to 200 pA) is plotted. Excitability was calculated as area under the curve. There was a significant effect of cell type on excitability ($F_4 = 25.08$, $p < .001$); excitability was lower in VGluT2+ cells relative to all other subtypes (ChAT: $t = 2.83$, $p = .011$; PV: $t = 6.62$, $p < .001$; GABA type I:

$t = 3.57$, $p = .001$; GABA type II: $t = 2.20$, $p = .034$). **(D)** Representative trace demonstrating spontaneous firing rate and waveform of genetically identified VP subpopulations. Scale bars for action potential trace: 10 mV, 20 ms. Scale bars for spontaneous activity trace: 10 mV, 1 s.

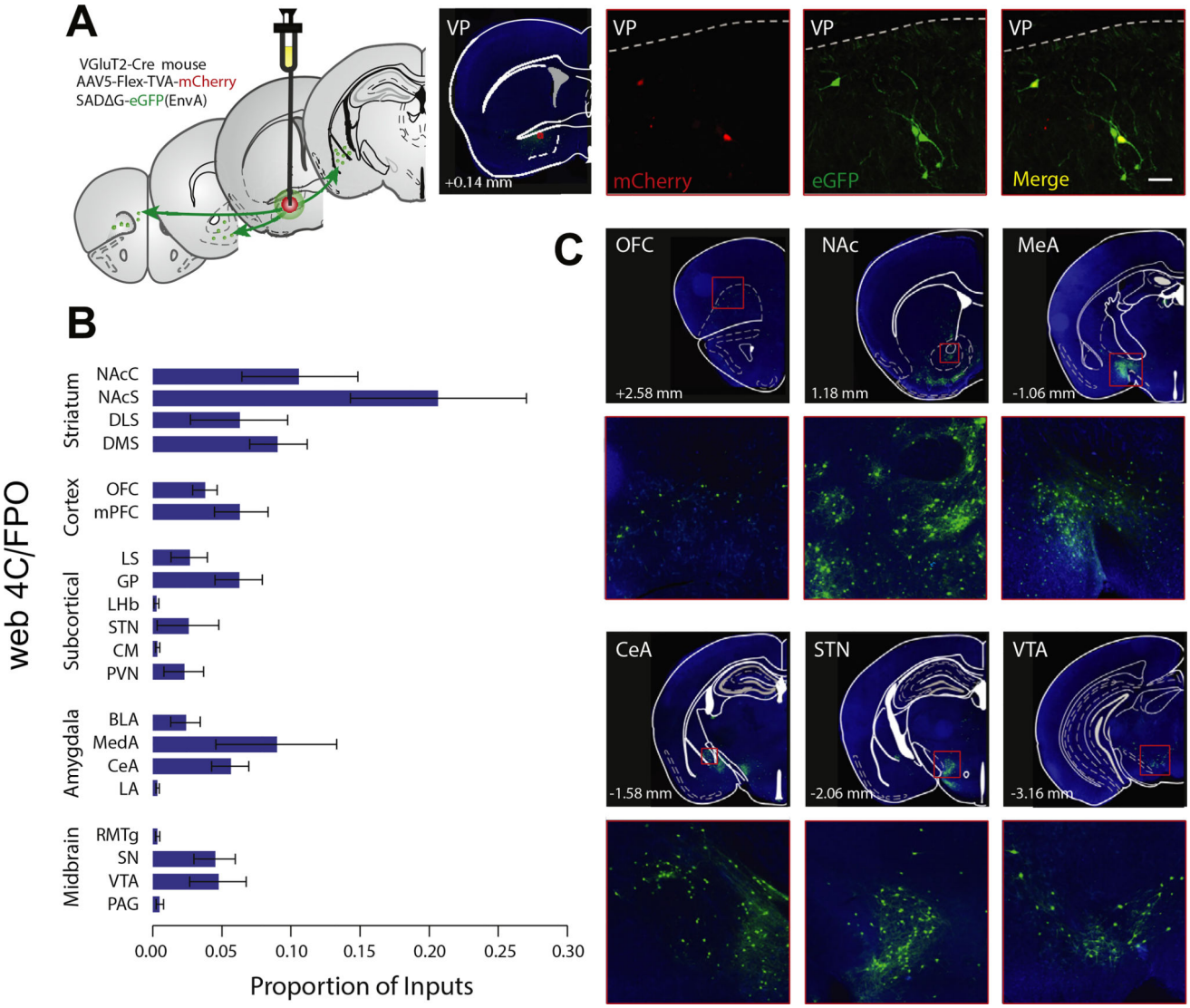

Figure 3.

Pseudorabies tracing reveals monosynaptic inputs to glutamatergic ventral pallidum (VP) neurons. **(A)** Experimental schematic. Floxed adeno-associated virus constructs encoding the rabies G protein and envelope protein, followed by the G-deleted pseudorabies virus encoding green fluorescent protein (eGFP), were injected into the VP of VGluT2-Cre mice to map monosynaptic inputs to the VP. A confocal image of example starter cells expressing mCherry and GFP is shown. **(B)** GFP-positive cells were quantified in striatal, cortical, subcortical, and amygdala subregions and midbrain areas and expressed as a proportion of total GFP-positive cells (see Supplemental Table S1). **(C)** Representative pictomicrographs (4×) and insets (20×) showing GFP-labeled cells in the orbitofrontal cortex (OFC) (top left), nucleus accumbens core (NAc) and striatum (top center), medial amygdala (MeA) (top right), central amygdala (CeA) (bottom left), subthalamic nucleus (STN) (bottom center), and ventral tegmental area (VTA) (bottom right). Scale bar = 100 μM. BLA, basolateral amygdala; CM, central medial nucleus; DLS, dorsolateral striatum; DMS, dorsomedial striatum; GP, globus pallidus; LA, lateral amygdala; LHb, lateral habenula; LS, lateral

septum; mPFC, medial prefrontal cortex; NAcS, nucleus accumbens shell; PAG, periaqueductal gray; PVN, paraventricular thalamus; RMTg, rostromedial tegmentum; SN, substantia nigra.

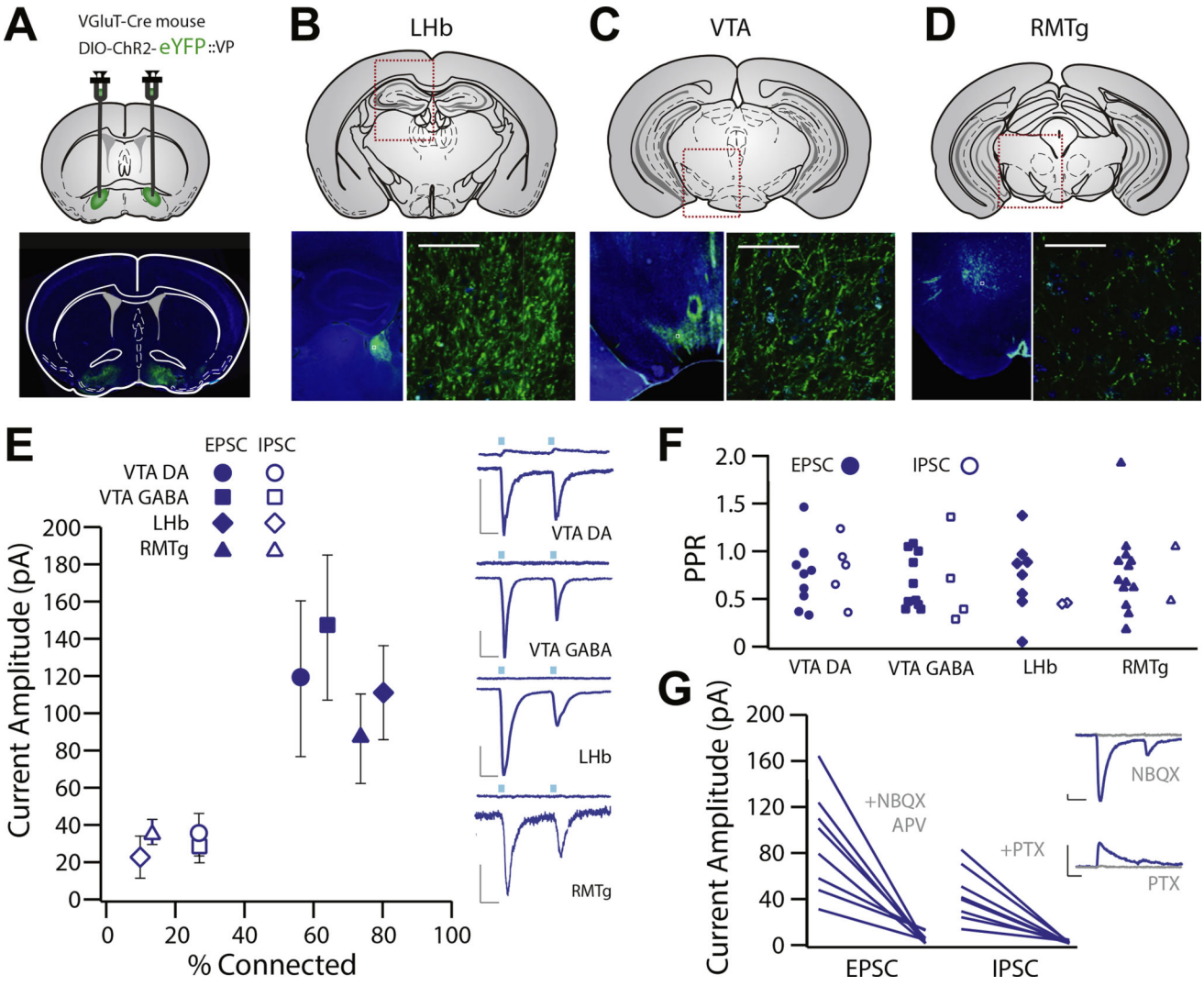

Figure 4.

Glutamatergic ventral pallidum (VP) neurons exhibit functional projections to the lateral habenula (LHb), ventral tegmental area (VTA), and rostromedial tegmental nucleus (RMTg). **(A–D)** Experimental schematic and widefield images showing floxed channelrhodopsin-2 (ChR2) with enhanced yellow fluorescent protein (eYFP) injection sites to the VP of VGluT2-Cre mice and terminal fields in the LHb **(B)**, VTA **(C)**, and RMTg **(D)**. **(E)** Patch clamp recordings were made of neurons in the terminal fields of vesicular glutamate transporter–positive VP neurons in the LHb (n = 20, capacitance = 17.63 ± 1.32 pF), RMTg (n = 15, capacitance = 26.83 ± 2.56 pF), and VTA (dopamine [DA] neuron n = 14, capacitance = 55.53 ± 5.097 pF, gamma-aminobutyric acid [GABA] neuron n = 14, capacitance = 19.96 ± 1.64). Recordings made at −70 mV revealed robust inward excitatory postsynaptic currents (EPSCs) (LHb: 80.0% connected, −89.7 ± 20.5 pA; RMTg: 73.3% connected, −98.6 ± 23.4 pA; VTA DA: 64.3% connected, −113.4 ± 43.4 pA; VTA GABA: 57.1% connected, −104.9 ± 40.6 pA), and recordings made at 0 mV revealed infrequent outward inhibitory postsynaptic currents (IPSCs) (LHb: 10% connected, 33.5 ± 19.6 pA; RMTg: 13.3% connected, 32.5 ± 5.5 pA; VTA DA: 42.8% connected, 31.8 ± 7.2 pA; VTA

GABA: 35.7% connected, 83.2 ± 44.6 pA). There was no difference between areas with respect to proportion of neurons exhibiting light-evoked currents, and EPSCs were observed more frequently than IPSCs [*t* test between proportions; VTA DA $\chi^2(1) = 1.25$, $p = .26$; VTA GABA $\chi^2(1) = 1.25$, $p = .26$; LHb $\chi^2(1) = 14.04$, $p < .001$; RMTg $\chi^2(1) = 10.63$, $p = .001$]. **(F)** There was no significant difference in EPSC or IPSC paired-pulse ratio (PPR) in any region (VTA DA: $t_4 = 0.6941$, $p = .5258$; VTA GABA: $t_3 = 0.2195$, $p = .8403$; LHb: $t_2 = 0.0187$, $p = .9867$; RMTg: $t_1 = 0.7603$, $p = .5862$) or in PPR between any brain region in terms of EPSC (one-way analysis of variance, EPSC $F_3 = 0.2552$, $p = .8572$; mean VTA DA = 0.637 ± 0.091, VTA GABA = 0.784 ± 0.139, LHb = 0.691 ± 0.122, RMTg = 0.654 ± 0.116) or IPSC amplitude (one-way analysis of variance, IPSC $F_3 = 0.2487$, $p = .8605$; VTA DA = 0.794 ± 0.166, VTA GABA = 0.849 ± 0.193, LHb = 0.620 ± 0.190, RMTg = 0.709 ± 0.265). **(G)** We verified that outward EPSCs were blocked by the combination of alpha-amino-3-hydroxy-5-methyl-4-isoxazole propionic acid and *N*-methyl-D-aspartate receptor antagonists (6-nitro-7-sulfamobenzoquinoxaline-2-3-dione [NBQX] and D, L-2-amino-5-phosphonovaleric acid [APV] at 100 μM), and outward IPSCs were blocked by the chloride channel blocker picrotoxin (PTX; 50 μM). Scale bars: 20 pA, 20 ms.

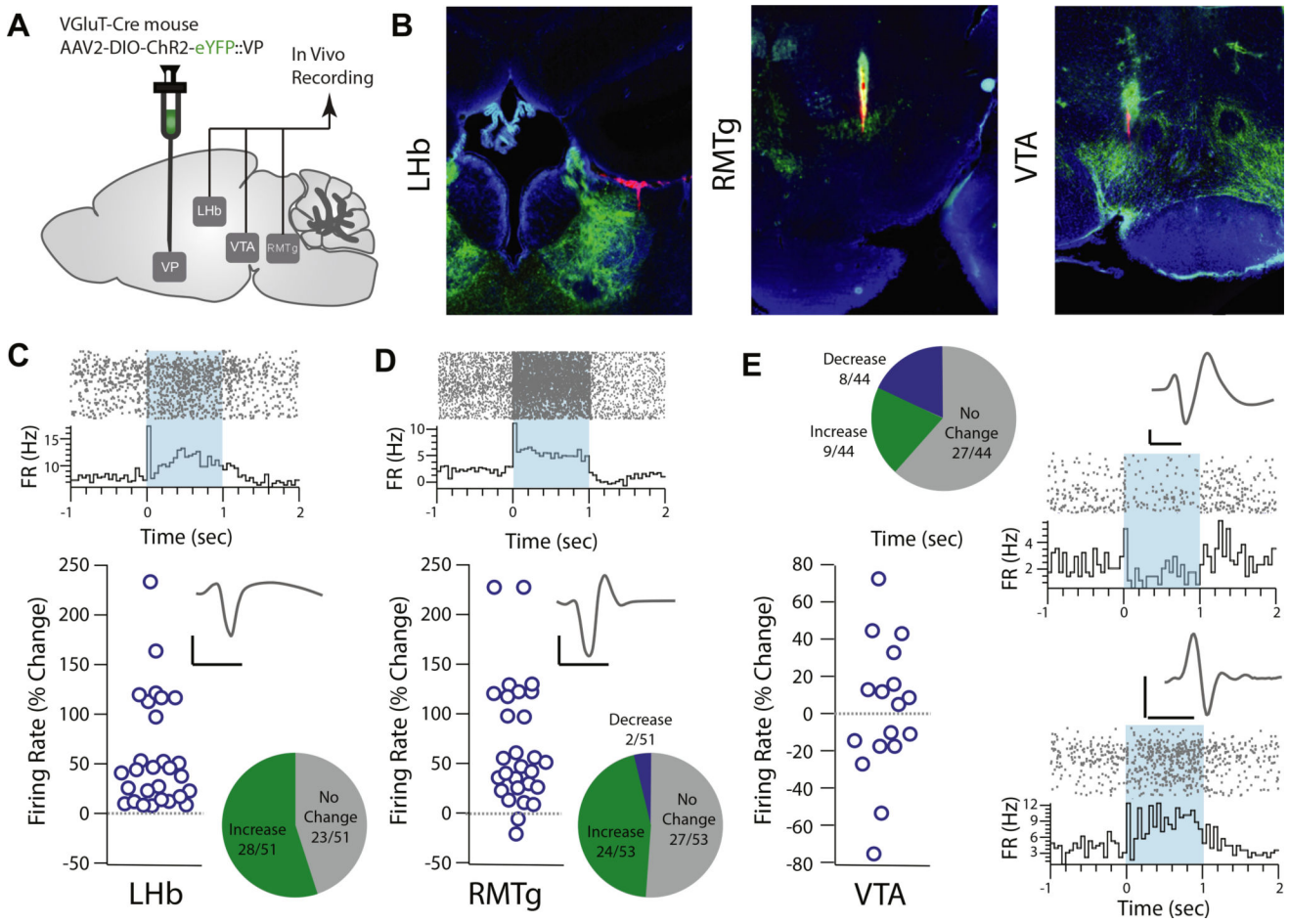

Figure 5.

Optogenetic activation of glutamatergic ventral pallidum (VP) neurons increases firing rates of lateral habenula (LHb) and rostromedial tegmental nucleus (RMTg) neurons and modulates ventral tegmental area (VTA) firing rates in vivo. **(A)** Experimental schematic. Floxed channelrhodopsin-2 (ChR2) with enhanced yellow fluorescent protein (eYFP) was injected into the VP of VGluT2-Cre mice, and in vivo recordings were performed in the LHb, RMTg, and VTA. **(B)** Representative images showing histological verification of recording sites in the LHb (left), RMTg (center), and VTA (right). **(C)** Representative recording from an isolated LHb unit (top; raster plot and peri-event histogram) aligned to onset of a 1-s optogenetic stimulation of vesicular glutamate transporter–positive VP neurons. Representative recording shows firing rate 1 s before optogenetic onset to 2 s following onset. Unit waveform is shown in inset. In total, 51 units were identified, 28 of which were significantly modulated, and all significantly modulated units exhibited an increased firing rate (45.1% unmodulated, 54.9% increased). The firing rate increased by 56.7 ± 11.8% in significantly modulated units. **(D)** Representative recording from an isolated unit from the RMTg. In total, 53 units were identified, 26 of which were significantly modulated (50.9% unmodulated, 45.3% increased, 3.8% decreased). Together, the firing rate of the RMTg increased by 61.55 ± 12.5% in significantly modulated units. **(E)** In the VTA, 44 units were identified; of these, 61.4% were unmodulated, 20.5% increased their firing

rate, and 18.2% decreased their firing rate in response to optogenetic activation of vesicular glutamate transporter–positive VP neurons. A representative triphasic waveform and raster plot from a negatively modulated unit (top) and a positively modulated unit (bottom) are shown. Scale bars: 20 μs, 20 mV. FR, firing rate.

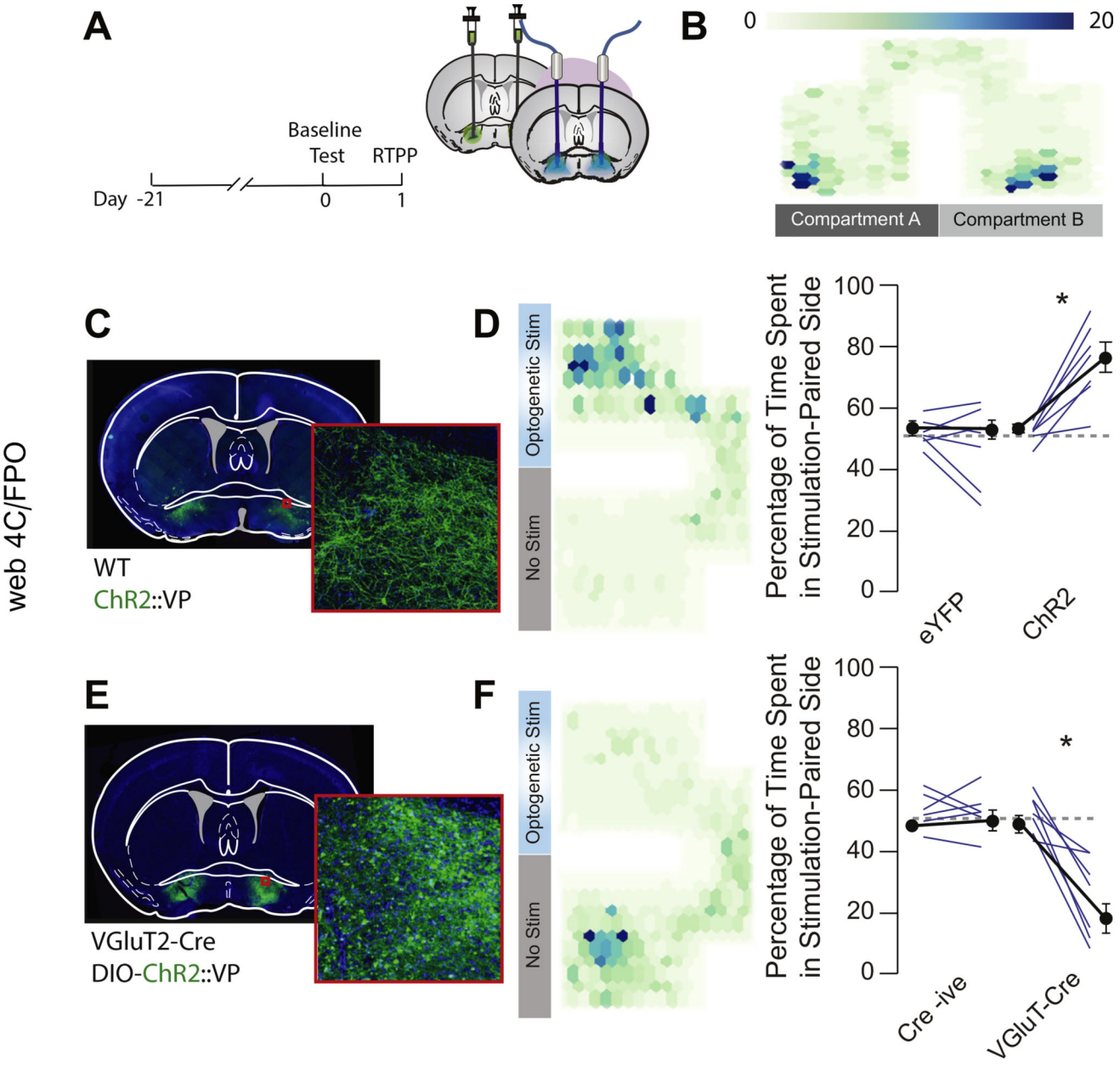

Figure 6.

Activation of glutamatergic ventral pallidum (VP) neurons induces real-time place aversion. **(A)** Experimental schematic. Unfloxed channelrhodopsin-2 (ChR2) was injected into the VP of wild-type (WT) mice, floxed ChR2 was injected into the VP of VGluT2-Cre mice, and optic fibers were implanted over the injection site. A baseline place preference task was conducted 24 hours before the real-time place preference (RTPP) task. **(B)** Representative heat map showing no baseline preference for either chamber of the test apparatus (scale indicates activity counts of tracked position). **(C)** Widefield image of infection site of unfloxed ChR2-enhanced yellow fluorescent protein (eYFP) in the VP. **(D)** Nonspecific optogenetic stimulation (stim) of the VP induced an RTPP (baseline 51.1 ± 1.4%, stim 77.1 ± 4.9%; $t_6 = 6.17$, $p < .001$), while stimulation with the control fluorophore had no effect

(baseline 49.7 ± 1.7%, stim 47.0 ± 5.1%; $t_6 = 1.036$, $p = .34$). **(E)** Widefield image showing infection site of floxed ChR2-eYFP in the VP of VGluT2-Cre mice. **(F)** Selective optogenetic activation of glutamatergic VP neurons induced a real-time place aversion (baseline 49.9 ± 2.8%, stim 23.1 ± 6.03%; $t_6 = 6.05$, $p < .001$), while Cre-negative littermates showed no response to light stimulation (baseline 53.1 ± 2.5%, stim 52.8 ± 3.1%; $t_5 = 0.11$, $p = .914$).

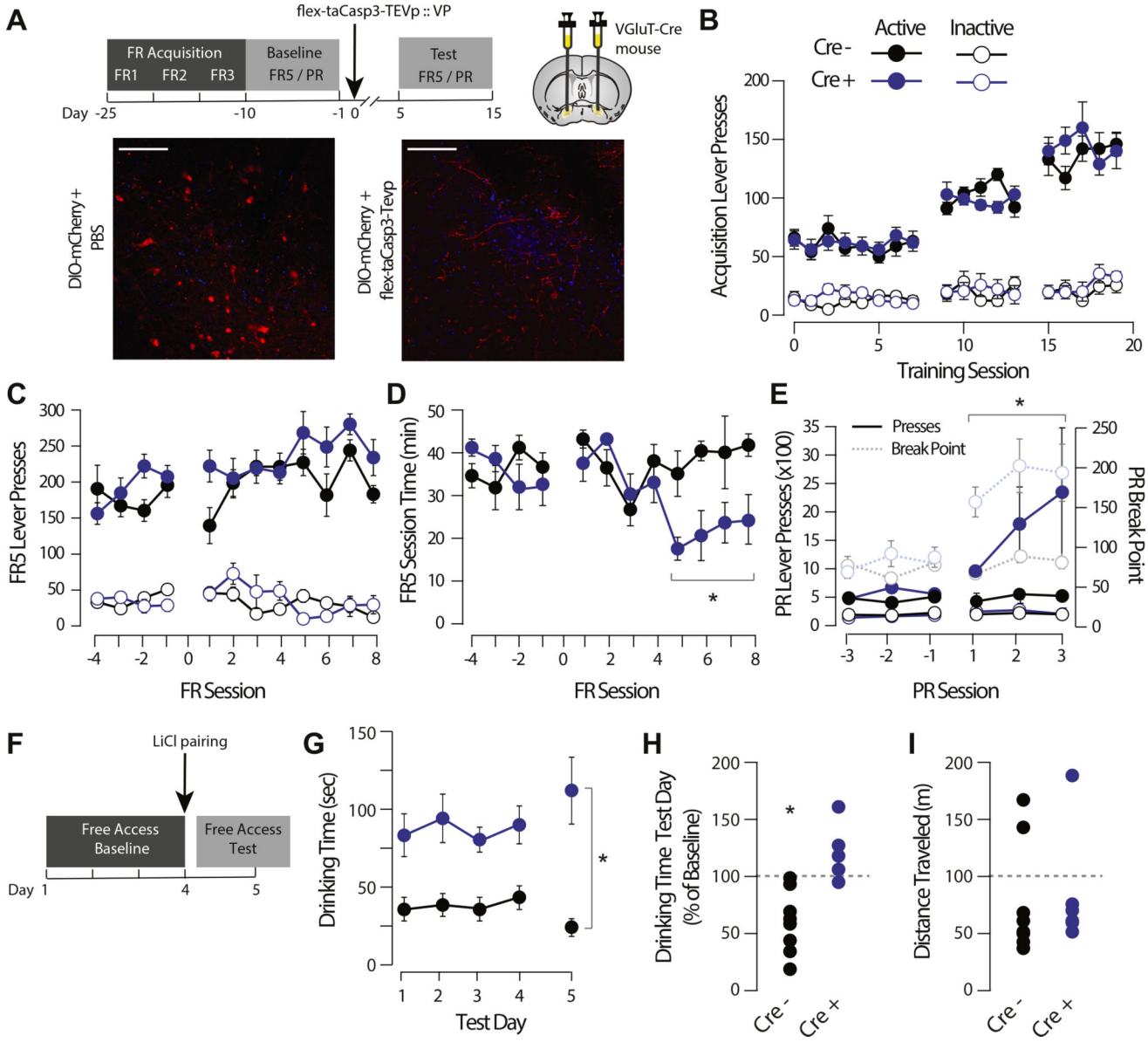

Figure 7.

Genetically encoded, caspase-mediated ablation of glutamatergic ventral pallidum (VP) neurons increases responding for sucrose and impairs sucrose taste aversion learning. **(A)** Experimental schematic. Mice were trained on an operant task to lever press for a sucrose pellet at fixed ratio (FR) 1 schedule. When performance stabilized on FR 1 responding, five sessions each of FR 2 and 3 schedules were completed before baseline operant testing (consisting of FR 5 and progressive ratio [PR] test sessions). VGluT2-Cre mice or Cre-negative control mice were then injected bilaterally with Cre-dependent viral caspase, and testing was resumed. Representative pictomicrographs showing floxed mCherry expression in the VP of unlesioned (left) and taCasp-lesioned (right) mice are shown. **(B)** There was no effect of genotype on the initial acquisition of the FR responding task ($F_{genotype}$ = 0.196, p = .662); lever presses increased as a function to FR schedule ($F_{session}$ = 314.117, p < .001), and there was a significant difference between active and inactive lever presses (F_{lever} =

281.999, $p < .001$). **(C)** There was no effect of lesion on number of FR 5 lever presses (Cre− = pre 197.83 ± 9.5, post 264.13 ± 12.4 presses/session; Cre+ = pre 183.78 ± 10.65, post 214.53 ± 10.8 presses/session; $F_{\text{session} \times \text{genotype}} = 2.612$, $p = .120$). **(D)** Following lesion, the amount of time to earn 30 sucrose rewards decreased in VGluT2-Cre mice (Cre− = pre 36.09 ± 1.9, post 39.36 ± 2.54 min/session; Cre+ = pre 36.12 ± 2.6, post 22.04 ± 2.31 min/session; $F_{\text{session} \times \text{genotype}} = 64.193$, $p = .003$). **(E)** Following lesion, the number of lever presses in the PR task increased in VGluT2-Cre mice (Cre− = pre 372.11 ± 28.14, post 443.39 ± 32.9 presses/session; Cre+ = pre 496.24 ± 48.87, post 1656.62 ± 444.88 presses/session; $F_{\text{session} \times \text{genotype}} = 5.198$, $p = .004$), as did the breakpoint (Cre− = pre 14.47 ± 0.38, post 15.0 ± 0.41, Cre+ = pre 15.2 ± 0.3, post 19.0 ± 0.42, $F_{\text{session} \times \text{genotype}} = 5.09$, $p = .001$). **(F)** Schematic of sucrose aversion task. Lesioned mice were given free access to sucrose solution over a 4-day baseline. Sucrose solution was then paired with lithium chloride (LiCl), and mice were retested the following day. **(G, H)** Absolute time spent drinking sucrose was higher in VGluT2-Cre-lesioned mice (84.8 ± 8.4 s/session) than in wild-type control mice (40.3 ± 4.6 s/session). Wild-type mice decreased their sucrose consumption following LiCl pairing (50.3 ± 11.1% decrease from baseline; t_7 paired t test = 2.844, $p = .0249$), whereas VGluT2-Cre-lesioned mice did not decrease their sucrose consumption in response to LiCl pairing (31.4 ± 9.4% nonsignificant change; t_5 paired t test = 1.9024, $p = .115$). There was a significant effect of genotype and day by genotype by day interaction ($F_{\text{genotype}} = 39.034$, $p < .001$; $F_{\text{genotype} \times \text{test}}$ day = 9.603, $p = .009$. **(I)** There was no difference in spontaneous locomotor activity between lesioned WT (82.7 ± 20.8 m) and VGLuT2-Cre (77.7 ± 17.5 m) mice in an open field arena task ($t_{12} = 0.184$, $p = .858$). Scale bar = 50 μM.